

Measurements of Piezoelectric Coefficient d_{33} of Lead Zirconate Titanate Thin Films Using a Mini Force Hammer

Qing Guo
Graduate Student

G. Z. Cao
Professor

Department of Material Science
& Engineering,
University of Washington,
Seattle, WA 98195-2120

I. Y. Shen¹
Professor

Department of Mechanical Engineering,
University of Washington,
Seattle, WA 98195-2600
e-mail: ishen@u.washington.edu

Lead zirconate titanate ($PbZr_xTi_{1-x}O_3$, or PZT) is a piezoelectric material widely used as sensors and actuators. For microactuators, PZT often appears in the form of thin films to maintain proper aspect ratios. One major challenge encountered is accurate measurement of piezoelectric coefficients of PZT thin films. In this paper, we present a simple, low-cost, and effective method to measure piezoelectric coefficient d_{33} of PZT thin films through use of basic principles in mechanics of vibration. A small impact hammer with a tiny tip acts perpendicularly to the PZT thin-film surface to generate an impulsive force. In the meantime, a load cell at the hammer tip measures the impulsive force and a charge amplifier measures the responding charge of the PZT thin film. Then the piezoelectric coefficient d_{33} is obtained from the measured force and charge based on piezoelectricity and a finite element modeling. We also conduct a thorough parametric study to understand the sensitivity of this method on various parameters, such as substrate material, boundary conditions, specimen size, specimen thickness, thickness ratio, and PZT thin-film material. Two rounds of experiments are conducted to demonstrate the feasibility and accuracy of this new method. The first experiment is to measure d_{33} of a PZT disk resonator whose d_{33} is known. Experimental results show that d_{33} measured via this method is as accurate as that from the manufacturer's specifications within its tolerance. The second experiment is to measure d_{33} of PZT thin films deposited on silicon substrates. With the measured d_{33} , we predict the displacement of PZT thin-film membrane microactuators. In the meantime, the actuator displacement is measured via a laser Doppler vibrometer. The predicted and measured displacements agree very well validating the accuracy of this new method. [DOI: 10.1115/1.4006881]

1 Introduction

MEMS actuators driven by lead zirconate titanate ($PbZr_xTi_{1-x}O_3$, or PZT) have received wide attention recently because they could potentially outperform other MEMS actuators in terms of bandwidth [1–3], energy density [4], and actuation strength. As a result, PZT microactuators enable various new advanced applications, such as minute hearing aids [5,6], miniaturized diagnostic tools [7,8], micropumps and microejectors [9,10], atomic force microscopy [11], head positioning system of optical and hard disk drives [12,13], and active control systems [14]. Moreover, PZT has been adopted in microsensors for many innovative applications, such as energy converters and harvesters [15–17], active and passive damage detection [18], and random access memory [19–21]. In scaling down the size to submillimeter range, PZT microsensors and microactuators often employ PZT thin films whose thickness is less than 10 μm to maintain a proper aspect ratio. The form of PZT thin films, however, presents a wide range of unique challenges that do not exist in bulk PZT or thick-film PZT (with film thickness more than 100 μm). One of them is measurement and calibration of piezoelectric coefficient d_{33} .

For bulk PZT or thick-film PZT, piezoelectric coefficient d_{33} is often measured in two ways. The first way is to apply an electric field and measure the corresponding strain. In this case, displacement of the PZT surface is often measured via a capacitive displacement probe [22], a laser interferometer [23] or a laser

Doppler vibrometer (LDV) [24]. Then the normal strain is calculated from the measured displacement.

These methods, however, become impractical for PZT thin films for several reasons. First, normal displacement of PZT thin films is extremely small due to their small thickness in comparison with that of bulk or thick-film PZT. This small displacement is often out of the resolution limit of displacement probes. As a result, the calculated normal strain suffers poor resolution and low signal-to-noise ratio. Second, laser interferometer measurements highly depend on surface quality of the PZT sample. The specimen has to be either polished or attached with a mirror to obtain a flat and reflective surface. This proves to be very difficult to realize, when PZT appears in the form of thin films. Third, the measurement of laser interferometer and LDV tend to include a large contribution from substrate bending and distortion, which cannot be accounted for accurately.

The second way to measure d_{33} for bulk or thick-film PZT is to apply a known force and measure the corresponding charge [25]. The applied forces can be either static or dynamic. If a static (i.e., constant) force is uniformly applied over a bulk or thick-film PZT specimen, the stress can be calculated from the applied constant force and the area over which the force is applied. In the meantime, the corresponding charge density can be obtained through the product of the capacitance and voltage of the PZT divided by the electrode area. Theoretically, in the time domain, d_{33} is the ratio between the charge density and the stress.

Alternatively, a dynamic force can be applied to a bulk or thick-film PZT specimen via a mechanical shaker [22], as typically done in d_{33} meters or charge measuring rigs. In this case, the instrument first applies a constant preload to hold the PZT specimen. Then it varies the applied load harmonically at an ac frequency that is above

¹Corresponding author.

Contributed by the Design Engineering Division of ASME for publication in the JOURNAL OF VIBRATION AND ACOUSTICS. Manuscript received April 20, 2011; final manuscript received April 2, 2012; published online February 4, 2013. Assoc. Editor: Wei-Hsin Liao.

the cutoff frequency of the PZT resistor-capacitor (RC)-circuit but below the resonance frequency of the specimen. In the instrument, a load cell measures the varying applied load and a charge amplifier records the charge. Then d_{33} can be calculated using the same method described above for the constant force measurement.

Both static and dynamic measurement methods become impractical for PZT thin films. In the case of static forces, PZT thin films often have a much smaller time constant than bulk or thick-film PZT. As a result, the measured charge decays very quickly and is difficult to measure accurately in the time domain. Moreover, as PZT becomes thin (e.g., 1 μm), the output voltage is significantly reduced and the signal-to-noise ratio drops. To reduce the noise, a very large force is needed in the measurements. The large force could, in turn, fracture or depolarize the PZT thin films [25].

In the case of d_{33} meters (i.e., dynamic forces), d_{33} meters frequently fracture PZT thin-film specimens when the static preload is applied. If the specimens survive the preload, d_{33} meters often penetrate the top electrode during the measurement phase due to the friction between the meter's probe and the specimen. Moreover, the measurements from d_{33} meters vary substantially from point to point on the same specimen (if the specimen survives the preload and the friction). This primarily results from the fact that thin-film specimens often take the form of a thin plate instead of a thick block. Consequently, dimensions, geometry, measurement locations, and boundary conditions of the specimen can significantly affect the measured results.

Aside from these "operational" difficulties, measurements of d_{33} from PZT thin films also have their own unique challenges. For example, piezoelectric coefficients of PZT thin films can vary significantly on residual stresses [26,27]. PZT thin films could easily be depolarized during testing when excessive forces are applied [25]. PZT thin films must be tested integrally with its substrate; therefore, the test results will bear certain dependence on the substrate's geometry, material properties, and boundary conditions [28].

Facing these challenges, researchers have been developing innovative methods to measure piezoelectric coefficients of PZT thin films [29–33]. One approach is to use simple instrumentation and subsequently correct the effects from the substrate. For example, Lefki and Dormans [29] apply a static force ranging from 0 to 20 N via a metallic tip with 1 mm² area to a PZT thin film integrated on a silicon substrate. In return, they measure responding charge Q from the PZT film, and calculate the charge-force ratio known as $d_{33}(\text{dp})$ in the paper. Since the substrate is present, the measured $d_{33}(\text{dp})$ is different from the true piezoelectric coefficient d_{33} of the PZT film. Alternatively, Al-Ahmad and Plana [30] applied two electric fields (parallel-mode and antimodes) to PZT thin films and measure the variation in capacitance due to the two opposite orientations of the bias voltage, from which the piezoelectric coefficient d_{33} are derived. Although this method is simple and straightforward, it relies on many assumptions (e.g., stress-free condition and $d_{33} = 2d_{31}$) and completely ignores the effects of substrate.

The second approach is to use advanced experimental setup to minimize the effects of the substrate. Park et al. [31] use pneumatic loading to induce electric charge to characterize d_{33} . The advantage of this method is that a uniform and noncontact force is applied via the pneumatic loading. This method, however, requires significant hardware (e.g., air chamber). Also, the seals (e.g., O-ring) used in the application could potentially induce in-plane stresses affecting the measured d_{33} . Park et al. also do not devise a solution to compensate for the effects of the substrate. Kholkin et al. [32] and Chao et al. [33] use a dual-beam scanning laser interferometer to measure thickness change ΔL of a PZT film induced by an electric field. The piezoelectric coefficient d_{33} is then derived using $d_{33} = \Delta L/V$, where V is the applied voltage. Although this method is very appealing, the experimental setup and instrument layout is complicated and expensive. According to the theory of piezoelectricity, the thickness change measured will contain displacement induced by the applied electrical field and responding in-plane stresses simultaneously.

From the discussion above, measurements of piezoelectric constant d_{33} of PZT thin films face two major challenges. The first challenge is to eliminate the effects of the substrate. Some of the existing methods only need simple experimental setups, but they cannot completely compensate for the effects of the substrate [29,30]. The other existing methods rely significantly on sophisticated experimental setups to minimize the effects of the substrate [31–33]. The second challenge is accuracy of the measured d_{33} . None of the existing literature [29–33] investigates the accuracy of their measured d_{33} . For example, if the measured d_{33} is used to design a PZT thin-film microactuator, how much will the designed actuator response differ from the actual actuator response measured in experiments?

Motivated by the challenges above, we present in this paper a simple and cost-effective way to measure piezoelectric coefficient d_{33} of PZT thin films. Aside from being simple and cost-effective, this new method has two unique features. First, it rigorously accounts for the effect of the substrate. Therefore, such a method is particularly favorable during microfabrication, where the piezoelectric coefficient can be quickly estimated to determine the quality of the fabricated PZT thin films. Second, it measures d_{33} accurately. Therefore, one can use it to design a PZT thin-film microdevice, and subsequently predict its response accurately.

The new method to measure d_{33} is a two-step process. The first step is to use a mini impact hammer (with a load cell) to excite the PZT film. During the excitation, the impulsive force is measured via the load cell and the responding charge of the PZT film is measured through a charge amplifier. The impulsive force has large enough amplitude to ensure a good signal-to-noise ratio, but not so much to cause depolarization of the PZT thin films. Since the impulsive force has extremely short duration (e.g., 200 μs), the discharge effect (i.e., the time constant effect) of the PZT circuit can be ignored. With this method, a digital oscilloscope and a charge amplifier will be sufficient to complete the measurements. At the end of the experiment, a charge-force ratio can be obtained precisely.

Similar to $d_{33}(\text{dp})$ measured by Lefki and Dormans [29], the charge-force ratio will significantly depend on substrate properties and dimensions. Therefore, the second step is to compensate for the effects of the substrate in order to extract the true piezoelectric coefficient d_{33} from the measured charge-force ratio. To do so, one can conduct a finite element analysis of the tested specimen to determine a calibration factor that relates the charge-force ratio to the true piezoelectric coefficient d_{33} .

For the rest of the paper, we will first present theoretical foundation and a finite element modeling to quantify the calibration factor. In addition, we will conduct a parametric study to understand how the calibration factor depends on various parameters, such as substrate material, boundary conditions, specimen size, specimen thickness, thickness ratio, and PZT thin-film material. We then explain the experimental setup and conduct two rounds of experiments to demonstrate the accuracy (and thus feasibility) of this method. The first round of experiments is to apply this new method to a disk resonator with thick-film PZT, whose d_{33} is known, to confirm its accuracy. In the second round of experiments, we apply the new method to a PZT thin film deposited on a silicon wafer, use the extracted d_{33} to predict displacement of a PZT thin-film membrane microactuator, and confirm the microactuator's displacement via a laser Doppler vibrometer. The close agreement between the predicted and measured actuator displacements thus proves the accuracy of the new method. Finally, we conclude the paper with a remark on residual stresses in PZT thin films.

2 Theoretical Foundation

The analysis below provides a theoretical foundation to justify the use of an impact force to measure piezoelectric coefficient d_{33} of a PZT thin film.

Let us consider an elastic substrate occupying semi-infinite domain in Fig. 1. The substrate carries a bottom electrode, above

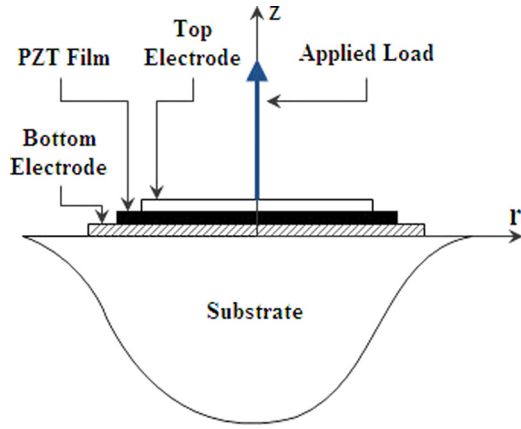


Fig. 1 Quasi-static analysis of substrate and PZT thin film

which a PZT thin film is coated. Finally, a top electrode occupying a finite area is deposited on the PZT film. The thickness of the two electrodes and PZT film is considered infinitesimal compared with the semi-infinite substrate; therefore, they do not contribute to any stiffness when the substrate deforms under external loads. The polar coordinates r and θ define the substrate surface, while coordinate z is normal to the substrate surface. In addition, $z=0$ defines the location of the two electrodes and the PZT film. Further, the electrodes are subjected to an open-circuit condition such that no net charge is flowing in or out of the electrode, i.e.,

$$q_3 = \int_A e_3 dA = 0 \quad (1)$$

where q_3 is the total charge out of the surface at $z=0$, e_3 is the electric displacement (i.e., charge density) in the z direction, and the integration can be over the top or bottom electrode.

Consider the case when an impulsive concentrated load $f(t) = F\delta(t)$ is applied at the origin in Fig. 1. Assuming a quasi-static condition, Boussinesq's solution of a semi-infinite half space in linear elasticity shows that the stresses on the surface at $z=0$ take the form of

$$\sigma_r = -\sigma_\theta = \frac{F(1-2\nu)}{2\pi r^2} \delta(t), \quad \sigma_{r\theta} = \sigma_{\theta z} = \sigma_{rz} = 0 \quad (2)$$

where σ_r, σ_θ are normal stresses, $\sigma_{r\theta}, \sigma_{\theta z}, \sigma_{rz}$ are shear stresses, and ν is the Poisson's ratio of the substrate. In addition, the normal stress σ_z is singular at $r=0$ satisfying

$$\int_A \sigma_z dA = F\delta(t) \quad (3)$$

In this case, the constitutive equation of the piezoelectricity $e_i = d_{ikl}\sigma_{kl} + \epsilon_{ik}E_k$ is reduced to

$$e_3 = d_{33}\sigma_z + d_{31}\sigma_r + d_{31}\sigma_\theta + \epsilon_{33}E_3 = d_{33}\sigma_z + \epsilon_{33}E_3 \quad (4)$$

where d_{33} is piezoelectric coefficient, ϵ_{33} is the dielectric constant, and E_3 is the electric field in the z direction. Note that the effect of d_{31} does not appear, because $\sigma_r = -\sigma_\theta$ from Eq. (2). Substitution of Eq. (4) into Eq. (1) results in

$$d_{33} = -\frac{\int_A \epsilon_{33}E_3 dA}{\int_A \sigma_z dA} \quad (5)$$

With a one-dimensional electrostatic analysis,

$$E_3 = V\delta(t)/d \quad (6)$$

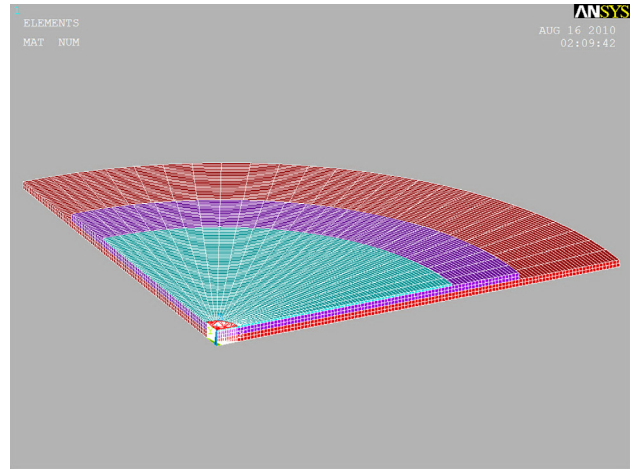


Fig. 2 Finite element model of circular disk resonator to determine α

where V is the voltage and d is the thickness of the PZT film. If we can assume that the PZT film behaves like a parallel capacitor, substitution of Eq. (3) and Eq. (6) into Eq. (5) to obtain

$$d_{33} = -\frac{C_{PZT}V}{F} \quad (7)$$

where $C_{PZT} = \int_A \frac{\epsilon_{33}dA}{d}$ is the capacitance of the PZT film. Note that F and V are the "strength" of the impact and responding voltage. For practical applications, they can be taken as the peak of the impact amplitude or the area underneath the impact history in the time domain.

Equation (7) rests on many critical assumptions that may not be realized in experiments. For example, a realistic specimen will not occupy a half-infinite space, and will be subjected to some sort of boundary conditions. The PZT thin film and electrodes will not have an infinitesimal thickness. The impact force applied will not be a point force; instead, it will have a spatial distribution. In light of these realistic constraints, Eq. (7) would take the form of

$$d_{33} = -\alpha \frac{C_{PZT}V}{F} \quad (8)$$

where α is a calibration factor associated with the specimen to be tested. If α is determined a priori via a finite element analysis, for example, Eq. (8) can be used to extract d_{33} experimentally free of the effects of the substrate. Also note that $C_{PZT}V/F$ is indeed the piezoelectric coefficient $d_{33}(dp)$ measured by Lefki and Dormans [29]. Extracting the true piezoelectric coefficient d_{33} will require a compensation of the substrate effects via the calibration factor α .

3 Effects of Substrate

To evaluate the calibration factor α for various substrates, we created several finite element models via ANSYS. Figure 2 shows a one-fourth model of a disk resonator. The disk resonator consisted of three layers: a brass substrate (also serving as the bottom electrode), a PZT thick film, and a top electrode. For the brass substrate, the diameter was 12 mm and thickness was 0.1 mm. It was meshed with solid elements. For the PZT thick film, the material properties are assumed to be PZT-5A. The diameter is 9 mm and the thickness is 0.1 mm. The PZT layer was meshed with piezoelectric solid elements. The top electrode was made of silver with diameter 7 mm and thickness 0.03 mm. It was also meshed with solid elements. The material properties of all layers are listed in Table 1 for reference.

Table 1 Material properties of all layers used in the finite element analysis for PZT thick-film specimen

	Reference model			Parametric studies		
	Top electrode (silver)	PZT-5A	Bottom electrode (brass)	Silicon	Glue layer	PZT-5H
Diameter (mm)	7	9	12	12	12	9
Thickness (μm)	30	100	100	100	50	100
ρ (kg/m^3)	1049	7750	8490	2330	1170	7500
d_{31} (m/V)		-1.71×10^{-10}				-2.74×10^{-10}
d_{33} (m/V)		3.74×10^{-10}				5.93×10^{-10}
d_{15} (m/V)		5.84×10^{-10}				7.41×10^{-10}
s_{11}^E (ms^2/kg)		1.64×10^{-11}				1.65×10^{-11}
s_{33}^E (ms^2/kg)		1.88×10^{-11}				2.07×10^{-11}
s_{12}^E (ms^2/kg)		-5.74×10^{-12}				-4.78×10^{-12}
s_{13}^E (ms^2/kg)		-7.22×10^{-12}				-8.45×10^{-12}
s_{44}^E (ms^2/kg)		4.75×10^{-11}				4.35×10^{-11}
s_{66}^E (ms^2/kg)		N/A				N/A
K_{11}^T		1730				3130
K_{33}^T		1700				3400
ϵ_0 (F/m)		8.85×10^{-12}				8.85×10^{-12}
E (GPa)	83		97	202	2.4	
ν	0.37		0.31	0.33	0.34	

The bottom nodes of the substrate were fixed in the space. Also, interfacial nodes between two adjacent layers were merged to ensure displacement continuity across the interfaces. At the center of the top electrode, a pressure load was applied normal to the electrode over a small area with a diameter of 0.61 mm (to simulate the contact area of a hammer tip to be used in experiments), while the rest of the top electrode was subjected to a stress-free boundary condition. The electric potential of the bottom electrode was set to zero, and the electric potential of the top electrode was assumed to be uniform. Note that the electric potential of the top electrode is unknown because it will depend on the charge generated from the impact force.

Figure 3 shows the charge $Q \equiv -C_{PZT}V$ generated in the PZT layer versus the applied force F . (It will be called “charge-force relationship” or simply Q - F curve for the rest of the paper.) The straight line with square solid markers is the ideal case depicted in Eq. (7), whose slope is the theoretical d_{33} of PZT-5A, which is 374 pC/N. The straight line with square open markers is from the finite element simulations of the disk resonator predicting a slope of 213 pC/N. As one can see, the finite element simulation does not predict the theoretical slope of d_{33} because the disk resonator specimen does not satisfy many assumptions made for Eq. (7). According to Eq. (8), the calibration constant of the circular disk resonator is

$$\alpha = \frac{374}{213} \approx 1.7559 \quad (9)$$

A parametric study was also conducted to find out what could significantly affect the calibration factor α from the reference configuration above. Parameters considered include substrate material, boundary conditions, specimen size, thickness, thickness ratio, and PZT thin-film material. The parametric study and its results are explained in detail as follows.

Substrate Material. The substrate material was changed from brass to silicon. Correspondingly, the Young’s modulus was changed from 97 GPa to 202 GPa; see Table 1 for detail. The resulting Q - F curve had a slope of 213 pC/N. Therefore, the substrate material almost does not affect the calibration factor α . To avoid confusion, this result is not presented in Fig. 3.

Boundary Conditions. In real experiments, the bottom of the substrate may be glued and is not subjected to a perfectly fixed boundary condition. To simulate this, a glue layer was introduced

in the finite element model between the substrate and the fixed boundary. The glue layer had a thickness of 0.05 mm and Young’s modulus of 2.4 GPa (Table 1). With the glue layer, the resulting Q - F curve had a slope of 225 pC/N, which leads to a calibration factor $\alpha = 374/225 \approx 1.6622$. This represents a minor 5.3% decrease from the calibration factor $\alpha \approx 1.7559$ in Eq. (9). To avoid confusion, this result is not presented in Fig. 3.

Specimen Size. In this study, the top electrode, PZT, and brass (bottom electrode) diameter of specimen were reduced from 7 mm to 3 mm, 9 mm to 5.5 mm, and 12 mm to 5.5 mm, respectively, while the thickness of each layer remained unchanged. The resulting Q - F curve has a slope of 200 pC/N, which leads to a calibration factor $\alpha = 374/200 \approx 1.8700$. This represents a minor 6.5% increase from the calibration factor $\alpha \approx 1.7559$ in Eq. (9). To avoid confusion, this result is not presented in Fig. 3.

Thickness Ratio. In this case, the overall thickness of the specimen remains unchanged, but the thickness ratio of the layers was altered. The thickness of the top electrode, PZT, and brass (bottom electrode) were changed to 0.3 μm , 0.673 μm , and 229.027 μm , respectively. In other words, both top electrode and PZT layer were roughly in the same order of magnitude, but were

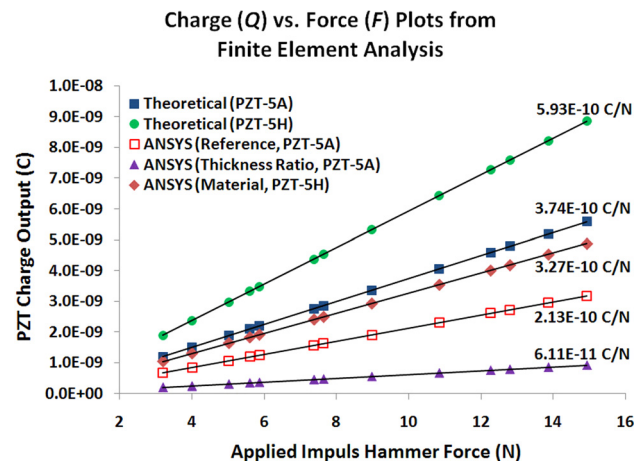


Fig. 3 Charge (Q) versus force (F) plots from finite element analysis

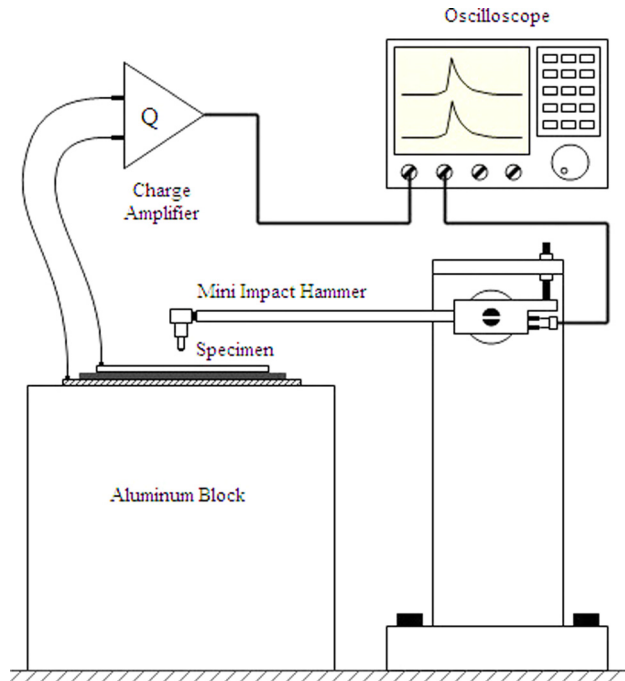


Fig. 4 Experimental setup

significantly thinner than the substrate. The resulting Q - F curve had a slope of 61 pC/N; see Fig. 3. This leads to a calibration factor $\alpha = 374/61 \approx 6.1311$, representing a significant 250% increase from the calibration factor $\alpha \approx 1.7559$ in Eq. (9).

Specimen Thickness. In this case, the thickness of the top electrode, PZT, and brass (bottom electrode) were reduced to 0.339 μm , 1.1313 μm , and 1.1313 μm , respectively. Note that the thickness ratio remains the same as that of the original reference system in Table 1. Yet the overall thickness was reduced to about 2.6 μm . The resulting Q - F curve had a slope of 223 pC/N, which leads to a calibration factor $\alpha = 374/223 \approx 1.6771$. This represents a minor 4.5% decrease from the calibration factor $\alpha \approx 1.7559$ in Eq. (9). To avoid confusion, this result is not presented in Fig. 3.

PZT Thin-Film Material. In this study, the material of PZT was changed to PZT-5H with theoretical d_{33} of 593 pC/N (Fig. 3). The resulting Q - F curve had a slope of 327 pC/N; see Fig. 3. This leads to a calibration factor $\alpha = 593/327 \approx 1.8135$ representing a minor 3.3% increase from the calibration factor $\alpha \approx 1.7559$ in Eq. (9).

The parametric study concludes that the calibration factor α is only sensitive to the thickness ratio. (In other words, the thickness ratio dominates the effects of the substrate.) This implies that the calibration factor α can be used to extract piezoelectric coefficient d_{33} , once the thickness ratio of each layer is determined in a specimen. The calibration factor α will be valid for a wide range of piezoelectric and substrate materials. Also, uncertainties in specimen size, thickness, and boundary conditions will not significantly affect the calibration factor α and thus the accuracy of this measurement method.

4 Experimental Setup and Validation

Figure 4 shows the experimental setup to instrument this new method. The setup consists of a mini impact hammer, a charge amplifier, an oscilloscope, and a specimen to be tested. The mini impact hammer (made by PCB Piezotronics, Model No. 086E80) has a metal tip with a diameter of 0.61 mm and a load cell with a calibration constant of 22. mV/N. When the hammer taps the specimen, the load cell measures the input force and the charge

amplifier measures the charge generated by the PZT. Both the measured force and charge are sent to the digital oscilloscope, where their peak amplitudes are recorded. Prior to the experiment, a finite element analysis was conducted to obtain the calibration factor α of the specimen. After the experiment, the piezoelectric coefficient d_{33} is calculated from the peak amplitudes and the calibration factor α according to Eq. (8).

To test the validity of this new approach, we first choose a thick-film PZT with a known d_{33} as our specimen. The specimen was a commercially available single-layered PZT disk resonator (made by APC International Ltd., Model No. MFT-12T-9.2A1). The disk resonator consisted of a brass disk (serving as the substrate and bottom electrode simultaneously), a thick-film PZT layer, and a silver top electrode on the PZT layer. The thickness of the brass disk, the PZT layer, and the silver electrode were 0.1 mm, 0.1 mm, and 0.03 mm, respectively. The diameter of the brass disk, the PZT layer, and the silver electrode were 12 mm, 9 mm, and 7 mm, respectively. The specimen was glued to a block of aluminum using epoxy to simulate a fixed boundary condition.

According to the manufacturer's specifications, the capacitance of the PZT film was $10 \pm 30\%$ nF and the film was made of PZT-5A. The exact value of d_{33} , however, was not listed in the specifications. Given a 30% tolerance in capacitance, we assume a 30% tolerance in d_{33} . Since the theoretical value of d_{33} for PZT-5A is 374 pC/N, the piezoelectric coefficient d_{33} of the disk resonator was estimated to be 374 ± 122 pC/N.

During the experiments, the vertical position of the hammer was finely adjusted so that a wide range of impact forces were applied to the specimen in order to obtain the charge-force relationship (i.e., the Q - F curve). For each hammer position, 20 taps were performed at the center of the specimen, and the peak amplitudes of the measured force and charge were averaged. Figure 5 shows some average force and charge measurements as an example. The top and bottom traces were measured force and charge, respectively. With the automatic hammer, the force level can be well controlled. Since 20 measurements were averaged, the measured force and charge are very consistent with very small noise.

After the force (F) and charge (Q) were measured, their peak values were substituted in Eq. (8). Also, the calibration factor α of the PZT thick-film specimen was 1.7559 from the finite element modeling discussed in Sec. 3. Then Eq. (8) calculates the piezoelectric coefficient d_{33} of the PZT thick film.

Three thick-film PZT specimens were tested. With $\alpha = 1.7559$, the calibrated charge-force relationship (i.e., αQ versus F) is plotted in Fig. 6. For each specimen, the markers are from the experimental measurements. The solid lines are from a least-square fit of the experimental measurements, whose slopes give the measured d_{33} according to Eq. (8). Also plotted in Fig. 6 is the theoretical charge-force relationship as a reference. The d_{33} obtained from this new approach for the three specimens is 457 pC/N, 426 pC/N, and 493 pC/N, respectively. Compared with the theoretical value 374 pC/N, the measurements from this approach are within the range of 14–32% difference, which is acceptable given that the variation of the specimen properties was 30%.

Throughout the experiments, a careful control the magnitude of the impact force was very important. We noticed that a too big impact force could result in depolarization of PZT thick film and affect the consistent d_{33} measurement.

5 Applications to PZT Thin Films

With the demonstrated feasibility of the new method on thick-film PZT, we then applied the new method to measure piezoelectric coefficient d_{33} of PZT thin films as follows.

A 3 in. wafer with a PZT thin film was fabricated using the following procedure. The silicon substrate (Si wafers with around 400 μm thickness) was first oxidized in a furnace at 1050 $^{\circ}\text{C}$ for 3 h to grow a SiO_2 layer of 500 nm thick. Then a layer of silicon nitride of 200 nm thick was deposited by LPCVD (low-pressure chemical vapor deposition). The bottom electrode consisted of

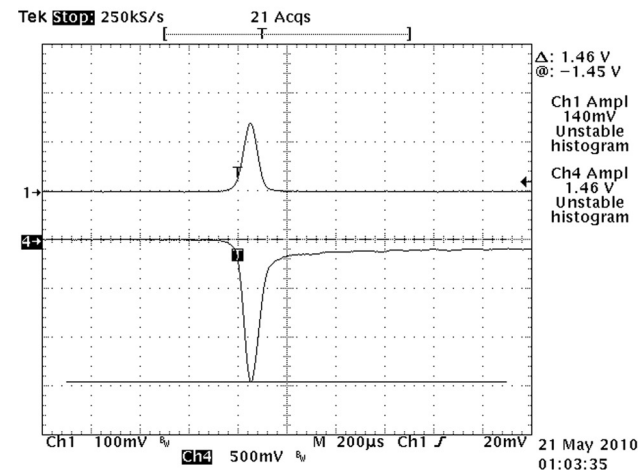
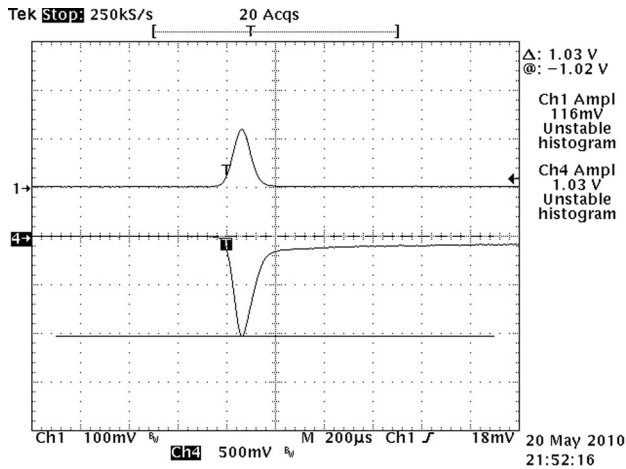


Fig. 5 Sample force and charge measurements in time domain for thick-film PZT specimen

Ti/Pt layers with thicknesses of 50 nm and 100 nm, respectively. The PZT film was spin-coated three times. For each coating, the sintering temperature was 650 °C for 15 min. For the third coating, the sol was diluted 50% by acetic acid and sintering temperature were reduced to 450 °C for 10 min. The thickness of the PZT film was measured around 1 μm. Next, the top electrode, consisting of Cr/Au layers (with a thickness of 25/500 nm) was deposited through evaporation. Moreover, the top electrode was patterned into multiple electrode pads with dimensions of 3 mm by 3 mm or 4 mm by 4 mm. After the fabrication was complete, the PZT film was poled with an electric field of 150 kV/cm at room temperature for 30 min. Finally, the wafer was diced into specimen with dimensions of 5.5 mm by 5.5 mm.

Based on the geometry described above, we created a finite element model of the thin-film PZT specimen. In Fig. 7, the finite element model is similar to that shown in Fig. 2, except that the model now has a separate substrate and bottom electrode. Moreover, the specimen is square instead of circular. Table 2 shows the material properties used in the finite element simulation for the PZT thin-film specimen. To obtain the calibration factor, we assume the PZT thin-film material to be PZT-7A with a theoretical piezoelectric constant d_{33} of 153 pC/N. The finite element analysis shows that the charge-force relationship for this specimen has a slope of 59.7 pC/N; see Eq. (8). Therefore, the calibration factor for the thin-film specimen is

$$\alpha = \frac{153}{59.7} \approx 2.5628 \quad (10)$$

Calibrated Charge-Force Relationship (αQ vs. F) from Experiments for Thick-Film PZT

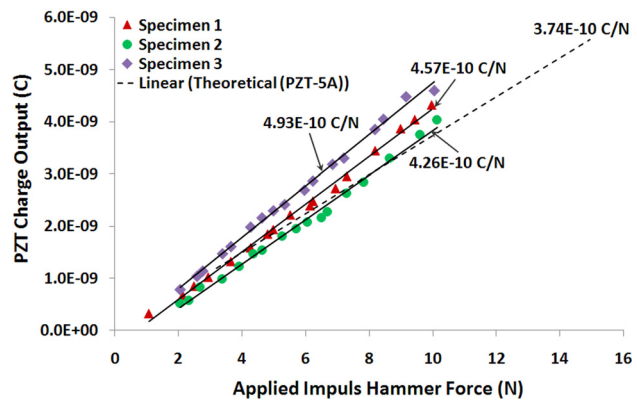


Fig. 6 Calibrated charge-force relationship (Q versus F) from experiments for thick-film PZT

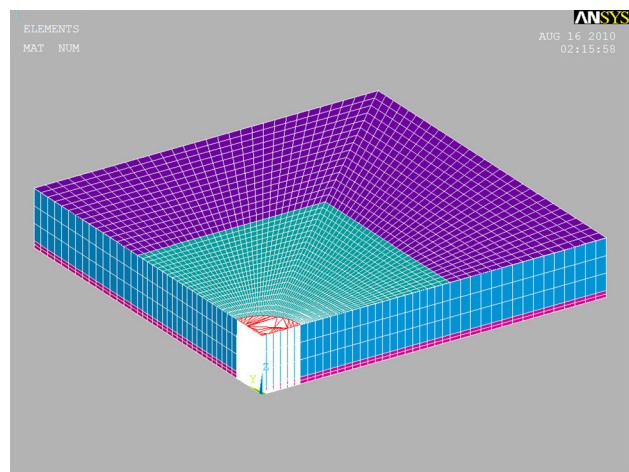


Fig. 7 Finite element model of thin-film PZT specimen

Two PZT thin-film specimens were tested using an impact force ranging from 1.8 N to 10 N. With $\alpha = 2.5628$, the calibrated charge-force relationship (αQ versus F) derived from the experiment is also added into Fig. 8 (cf. the triangular markers in Fig. 8). The open markers correspond to one specimen and the solid markers correspond to the second specimen. Since the experimental data from the two specimens are so consistent, only one solid line is used to least-square fit the data. The resulting slope of the least square fit is 21.3 pC/N, which is the measured d_{33} for the fabricated PZT thin film according to Eq. (8) free of the effects from the substrate.

There are several issues worth noting for these experimental measurements. First, the experimental measurements indicate that the fabricated PZT thin film has very uniform piezoelectric properties. The measurements from two separate specimens from the same wafer show almost the identical slope indicating very consistent d_{33} .

Second, the measured d_{33} from the PZT thin films is significantly less than that of bulk PZT-5A or PZT-7A. It is well known that piezoelectric coefficients of PZT thin films are smaller compared with those of bulk PZT due to small grain size of PZT film. Also, sol-gel derived PZT thin films will inherit residual stresses from their fabrication process, which subsequently affect the piezoelectric coefficients [26,27]. Therefore, we believe that the measured d_{33} in Fig. 8 is reasonable.

Table 2 Material properties of all layers used in the finite element analysis for PZT thin-film specimen

	Top electrode (gold)	PZT-7A	Bottom electrode (platinum)	Silicon	Glue layer
Length (mm)	3	5.5	5.5	5.5	5.5
Width (mm)	3	5.5	5.5	5.5	5.5
Thickness (μm)	0.5239	1.1313	0.2449	385.72	50
ρ (kg/m^3)	19280	7700	21450	2330	1170
d_{31} (m/V)		-0.60×10^{-10}			
d_{33} (m/V)		1.53×10^{-10}			
d_{15} (m/V)		3.60×10^{-10}			
s_{11}^E (ms^2/kg)		1.07×10^{-11}			
s_{33}^E (ms^2/kg)		1.39×10^{-11}			
s_{12}^E (ms^2/kg)		-3.58×10^{-12}			
s_{13}^E (ms^2/kg)		-4.60×10^{-12}			
s_{44}^E (ms^2/kg)		3.40×10^{-11}			
s_{66}^E (ms^2/kg)		2.86×10^{-11}			
K_{11}^T (unitless)		1354			
K_{33}^T (unitless)		617			
ϵ_0 (F/m)		8.85×10^{-12}			
E (GPa)	80		168	202	2.4
ν	0.42		0.38	0.33	0.34

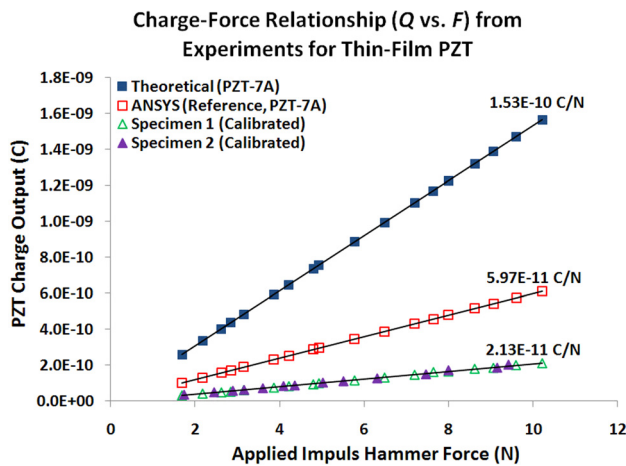


Fig. 8 Charge-force relationship (Q versus F) from experiments for thin-film PZT

Third, it is informative to compare how thick-film PZT and thin-film PZT behave differently to broaden our knowledge base. Table 3 lists major dimensions and measured properties of thick-film and thin-film PZT specimens. Although the capacitance of PZT thin film is larger than that of the thick-film PZT (19.3 = nF versus 9.02 nF), dielectric constant and piezoelectric coefficient of the PZT thin film are about one-order-of-magnitude smaller than those of the thick-film PZT (274.15 versus 2646.77 and 21.3 pC/N versus 457 pC/N, respectively). These results make sense, because the PZT thin films are fabricated using a sol-gel process. After sintering, PZT thin films are likely to become porous degrading the material properties. Also, a porous bottom electrode could greatly reduce the PZT thin film poling effectiveness yielding a low piezoelectric coefficient. In general, a reduction in dielectric constants often accompanies a reduction in piezoelectric coefficient.

6 Applications to PZT Thin-Film Microactuators

The measured d_{33} can now be used to design the PZT thin-film membrane microactuator shown in Fig. 9. The microactuator consists of four parts: a membrane, a bulk silicon substrate, a PZT thin-film layer, and a pair of electrodes. (Note that the parts in Fig. 9 are not drawn in proportion.) The membrane is a moving component of the actuator anchored to the silicon substrate. As a

Table 3 Comparison of dimensions and properties of thick-film and thin-film PZT specimens

	Thick-film PZT specimen	Thin-film PZT specimen
PZT size A_0 (mm^2)	63.617	30.25
Electrode size A (mm^2)	38.485	9
PZT thickness d (μm)	100	1.1313
Capacitance C (nF)	9.015	19.30
Dielectric constant ϵ_r	2646.773	274.15
Force voltage V_{in} (mV)	200	206
PZT voltage V_{out}	2.08 V	74 mV
d_{33} with correction factor (pC/N)	426–493	21.3

where dielectric constant $\epsilon_r = (Cd/\epsilon_0 A)$ with $\epsilon_0 = 8.854 \times 10^{-12} \text{C}^2/\text{m}^2\text{N}$

result of its small thickness, the silicon membrane has low structural stiffness compared with the substrate. Often, the membrane can be fabricated by releasing part of the bulk silicon substrate, for example, using deep reactive ion etch (Oxford Instruments ICP 380). On top of the membrane is a layer of PZT thin film with a pair of electrodes. When a driving voltage is applied to the electrodes, the PZT thin film extends or contracts in the plane of the membrane; thus creating a bending moment to flex the membrane out of its plane.

Lee et al. [34] has studied the PZT thin-film membrane actuator extensively. Experimentally, they measure the actuator displacement using a laser Doppler vibrometer. They also measured actuator dimensions using SEM. Numerically, they predict the actuator displacement using piezoelectric constants from bulk PZT-7A. The numerical predictions, however, disagree with the experimental measurements by an order of magnitude. As a result, Ref. [34] by Lee et al. serves as an ideal proving ground to validate the accuracy of the newly measured d_{33} in Sec. 5.

As a demonstration, let us focus on the actuator C4 described in Ref. [34]. The dimensions and natural frequencies of actuator C4 are listed in Table 4. The dimensions include the thickness of each layer in the actuator. Two natural frequencies are cited in Table 4. One is the natural frequency measured in the experiment, which is 59.578 kHz. The other is the natural frequency calculated via finite element analyses, which assume a PZT thin film with Young's modulus of 70 GPa and $d_{33} = 21.3$ pC/N measured in Sec. 5. The corresponding calculated is 40.942 kHz. Figure 10 shows measured displacement of actuator C4 with respect to the applied voltage. The response becomes nonlinear when the applied voltage is greater than 4 V. If the measured d_{33} in Sec. 5

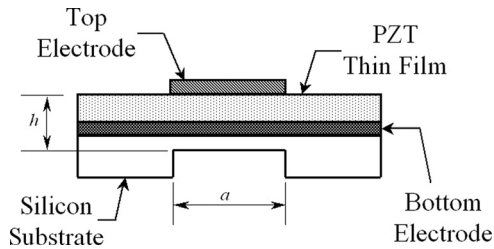


Fig. 9 Schematic drawing of PZT thin-film membrane actuator

is accurate, it will predict the measured actuator displacement below 4 V.

To predict the displacement of actuator C4 reasonably, two additional factors must be included: residual stresses and dimension variations. They are explained in detail as follows.

Significant residual stresses develop in the PZT thin-film membrane actuators. Since PZT is sintered at 650 °C and subsequently cooled down to room temperature, mismatch in coefficients of thermal expansion in different layers results in significant residual stresses. The in-plane residual stresses stiffen the membrane significantly increasing the natural frequency of the actuator. (That is why is greater than in Table 4.) Although the magnitude of the residual stresses is unknown, its effects on displacement reduction can be estimated via $\beta \equiv (\omega_{FEA}/\omega_{EXP})^2$. This is because natural frequency ω is proportional to \sqrt{k} , where k is the stiffness of the actuator. In addition, the actuator displacement is proportional to k^{-1} . Therefore, displacement predictions from finite element analyses must be multiplied by the factor $\beta \equiv (\omega_{FEA}/\omega_{EXP})^2$ to compensate for the stiffness increase caused by the residual stresses. For actuator C4, the correction factor is $\beta \equiv (\frac{40.942}{59.578})^2 \approx 0.4722$.

The thickness of each layer, as measured from SEM, bears an uncertainty too. The dimensions listed in Table 4 are measured so that the SEM is perpendicular to the Au layer. If the SEM is oriented such that it is perpendicular to the Si/SiO₂/SiN_x layer, the measured dimensions can vary by 10% to 20%.

With the information above, Fig. 10 shows the finite element analysis (FEA) displacement predictions using the measured d_{33} from Sec. 5 (i.e., 23.1 pC/N), correction factor $\beta \equiv (\omega_{FEA}/\omega_{EXP})^2$ for the residual stresses (i.e., 0.4722), and 20% variations in measured dimensions of each layer. The dash lines delineate the boundaries when the dimensions of each layer are varied. The measured actuator displacement below 4 V is within the boundaries proving that the measured d_{33} from Sec. 5 is accurate.

7 Remarks on Residual Stresses and Effects of d_{31}

For PZT thin films, presence of residual stresses can affect the piezoelectric coefficient d_{33} [26,27]. In other words, piezoelectric coefficient d_{33} is a function of residual stresses. Technically speaking, existing methods [29–33] all measure piezoelectric coefficient d_{33} of PZT thin films with residual stresses. Naturally,

Table 4 Layered structure thickness of the selected PZT actuator membrane

Actuator	C4
Si/SiO ₂ /Si ₃ N ₄	0.48 μ m
Ti/Pt	0.19 μ m
PZT	1.00 μ m
Au	0.53 μ m
Natural frequency (experiment)	59.578 kHz
Natural frequency (FEA, PZT-7A)	40.942 kHz
$\beta \equiv (\omega_{FEA}/\omega_{EXP})^2$	0.4722

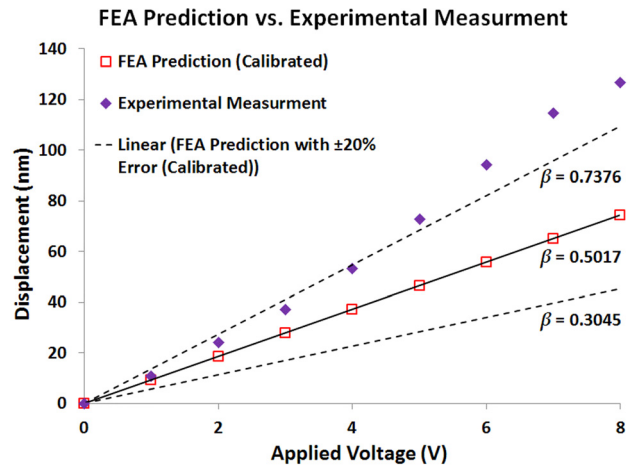


Fig. 10 Calibrated displacement-voltage relationship ($\beta \times$ versus V) from experiments for PZT thin-film actuator

the following two questions arise. First, does it make sense to measure piezoelectric coefficient d_{33} under the influence of residual stresses? Should one measure piezoelectric coefficient d_{33} , while the PZT film is under a stress-free condition? Second, does the new method presented in this paper remain valid, given that the finite element model does not include any residual stresses?

In so far as the first question, it actually makes more sense to measure piezoelectric coefficient d_{33} while residual stresses are present. When the PZT thin film is in use as a sensor or an actuator, the PZT thin film remains in the state of residual stresses. Therefore, measuring d_{33} with residual stresses will better match the condition that appears in actual devices. As such, the measured d_{33} with residual stresses can be used directly in finite element analyses to improve design or estimate performance of the sensor or actuator.

For the second question, the finite element modeling in Sec. 3 remains valid for thin films with embedded residual stresses. One should note that residual stresses could affect piezoelectric response as well as mechanical response. The finite element analysis in Sec. 3 aims to extract d_{33} from piezoelectric response to account for the effects of residual stresses. The effects of residual stresses on mechanical response should be accounted for via the correction factor $\beta \equiv (\omega_{FEA}/\omega_{EXP})^2$ at the device level.

Although d_{31} does not appear explicitly in this paper, effects of d_{31} are implicitly incorporated in this approach. Since the Boussinesq's solution cannot be realized in experiments, the correction factor α will depend not only on substrate parameters (e.g., thickness and material properties) but also on other piezoelectric constants of the film, such as d_{31} and d_{15} . When a bulk PZT material is chosen to create a reference finite element model, all its piezoelectric constants including d_{33} , d_{31} , and d_{15} are used. As the experimentally measured charge is compared with the finite element predictions to calibrate the correction factor α , it implies that the PZT film has the same d_{33} -to- d_{31} and d_{33} -to- d_{15} ratios as those of the bulk PZT used in the finite element predictions. Therefore, effects of d_{31} and d_{15} are included in this method, but d_{31} and d_{15} cannot be determined independently from this method.

8 Conclusions

In this paper, we have developed and demonstrated a simple and low-cost method to measure piezoelectric coefficient d_{33} of PZT thin films. The method adopts a mini-impact hammer to generate an impulsive force. A load cell at the tips of the hammer measures the impulsive force, and a charge amplifier measures the charge generated by the PZT layer. Prior to the experiment, a finite element analysis is conducted to estimate a calibration constant to compensate for the substrate effects associated with the

specimen. From the measured force and charge and the calculated calibration constant, we can estimate the piezoelectric coefficient d_{33} according to Eq. (8).

Experimental results on thick-film PZT specimens with known piezoelectric coefficients indicate that the method is accurate. Piezoelectric coefficient d_{33} measured using the new method is well within the specification tolerance. The method also works successfully on PZT thin films without damaging the films. Nevertheless, impact force level needs to be capped to avoid depolarization of the PZT thin films. With the measured d_{33} , we can predict the displacement of PZT thin-film membrane actuators accurately to match with existing experimental results.

This new method is distinct from existing measurement methods [29–33] in two aspects. First, it does not require expensive experimental setup, and yet it can accurately compensate for the effects of the substrate. It employs impact forces and averaging techniques. As a result, the measured data do not scatter and have very low noise level. Second, this paper proves that the measured d_{33} is accurate. Simulations based on the measured d_{33} predict the displacement of PZT thin-film membrane microactuators accurately.

Acknowledgment

This material is based upon work supported by the National Science Foundation under Grant No. CMMI-0826501.

References

- Zhang, Q. Q., Djuth, F. T., Zhou, Q. F., Hu, C. H., Cha, J. H., and Shung, K. K., 2006, "High Frequency Broadband PZT Thick Film Ultrasonic Transducers for Medical Imaging Applications," *Ultrasonics*, **44**, pp. 711–715.
- Guo, W., Wang, Z., Yao, X., Huang, T., and Bi, C., 1998, "A High Bandwidth Piezoelectric Suspension for Track Density Magnetic Data Storage Devices," *IEEE Trans. Magn.*, **34**(4), pp. 1907–1909.
- Wu, C.-C., Lee, C.-C., Cao, G. Z., and Shen, I. Y., 2006, "Effects of Corner Frequency on Bandwidth and Resonance Amplitude in Designing PZT Thin-Film Actuators," *Sensor. Actuat. A-Phys.*, **125**(2), pp. 178–185.
- Wood, R. J., Steltz, E., and Fearing, R. S., 2005, "Optimal Energy Density Piezoelectric Bending Actuators," *Sensor. Actuat. A-Phys.*, **119**(2), pp. 476–488.
- Fischer, M., and Niederdrank, T., 2004, "Micromechanical Piezoelectric Actuator for Hearing Aid Application," *ACTA Acust. United Ac.*, **90**(5), pp. 868–872.
- Lee, C.-C., Guo, Q., Hume, C. R., Cao, G. Z., and Shen, I. Y., 2007, "Electrode Optimization of PZT Thin-Film Microactuators for Hybrid Cochlear Implants," Abstracts of 2007 Conference on Implantable Auditory Prostheses, July 15–20, Lake Tahoe, CA.
- Chang, F. K., Markmiller, J. F. C., Ihn, J. B., and Cheng, K. Y., 2007, "A Potential Link From Damage Diagnostics to Health Prognostics of Composites Through Built-In Sensors," *ASME J. Vib. Acoust.*, **129**(6), pp. 718–729.
- Zhao, X., Qian, T., Mei, G., and Kwan, C., 2007, "Active Health Monitoring of an Aircraft Wing With an Embedded Piezoelectric Sensor/Actuator Network: II. Wireless Approaches," *Smart Mater. Struct.*, **16**(4), pp. 1218–1225.
- Chen, S. C., Cheng, C. H., and Lin, Y. C., 2007, "Fabrication of Components for a Valve-Less Micropump or Microejector by Multilevel Electroforming Technology," *Microsyst. Technol.*, **13**(5–6), pp. 455–463.
- Wang, D. A., Cheng, C. H., Hsieh, Y. H., and Zhang, Z. X., 2007, "Analysis of an Annular PZT Actuator for a Droplet Ejector," *Sensor. Actuat. A-Phys.*, **137**(2), pp. 330–337.
- Shibata, T., Unno, K., Makino, E., and Shimada, S., 2004, "Fabrication and Characterization of Diamond AFM Probe Integrated With PZT Thin Film Sensor and Actuator," *Sensor. Actuat. A-Phys.*, **114**(2–3), pp. 395–405.
- Yang, W., Lee, S. Y., and You, B. J., 2010, "A Piezoelectric Actuator With a Motion-Decoupling Amplifier for Optical Disk Drives," *Smart Mater. Struct.*, **19**(6), p. 065027.
- He, Z. M., Loh, H. T., and Ong, E. H., 2008, "Reliability Evaluation of Piezoelectric Micro-Actuators With Application in Hard Disk Drives," *IEEE Trans. Magn.*, **44**(11), pp. 3722–3725.
- Jarzyna, W., Augustyniak, M., and Bochenki, M., 2010, "Active Piezoelectric Structures in Control Systems," *Przeład Elektrotechniczny*, **86**(4), pp. 252–255.
- Chen, X., Xu, S., Yao, N., and Shi, Y., 2010, "1.6V Nanogenerator for Mechanical Energy Harvesting Using PZT Nanofibers," *Nano. Lett.*, **10**(6), pp. 2133–2137.
- Shen, D., Park, J., Noh, J., Choe, S., Kim, S., Wickle, H., and Kim, D., 2009, "Micromachined PZT Cantilever Based on SOI Structure for Low Frequency Vibration Energy Harvesting," *Sensor. Actuat. A-Phys.*, **154**(1), pp. 103–108.
- Li, Y., Li, W., Guo, T., Yang, Z., Fu, X., and Hu, X., 2009, "Study on Structure Optimization of a Piezoelectric Cantilever With a Proof Mass for Vibration-Powered Energy Harvesting System," *J. Vac. Sci. Technol. B*, **27**(3), pp. 1288–1290.
- Ou, J., and Li, H., 2010, "Structural Health Monitoring in Mainland China: Review and Future Trends," *Struct. Health Mon.*, **9**(3), pp. 219–231.
- Zhang, M., Jia, Z., and Ren, T., 2009, "Effects of Electrodes on the Properties of Sol-Gel PZT Based Capacitors in FeRAM," *Solid State Electron. Lett.*, **53**(5), pp. 473–477.
- Song, S., Song, Z., Liu, B., Wu, L., and Feng, S., 2010, "Ge₂Sb₂Te₅ and PbZr_{0.30}Ti_{0.70}O₃ Composite Films for Application in Phase Change Random Access Memory," *Mater. Lett.*, **64**(3), pp. 317–319.
- Miyake, M., Scott, J. F., Lou, X. J., Morrison, F. D., Nonaka, T., Motoyama, S., Tatsuta, T., and Tsuji, O., 2008, "Submicron Three-Dimensional Trenched Electrodes and Capacitors for DRAMs and FRAMs: Fabrication and Electrical Testing," *J. Appl. Phys.*, **104**(6), p. 064112.
- Dargie, P. G., Harris, N. R., White, N. M., Atkinson, J. K., and Sion, R. P., 2007, "Characterisation of Screen Printable Piezoelectric Thick-Films," Proceedings of the Eighth Conference on Sensors and Their Applications, September 7–10, Glasgow, UK.
- Zhang, Q. M., Pan, W. Y., and Cross, L. E., 1988, "Laser Interferometer for the Study of Piezoelectric and Electrostrictive Strains," *J. Appl. Phys.*, **63**(8), pp. 2492–2496.
- Rittenmyer, K., and Dubbelday, P., 1992, "Direct Measurement of the Temperature-Dependent Piezoelectric Coefficients of Composite Materials by Laser Doppler Vibrometry," *J. Acoust. Soc. Am.*, **91**(4), pp. 2254–2260.
- Li, F., and Fang, D., 2005, "Effects of Electrical Boundary Conditions and Poling Approaches on the Mechanical Depolarization Behavior of PZT Ceramics," *Acta Mater.*, **53**(9), pp. 2665–2673.
- Berfield, T. A., Ong, R. J., Payne, D. A., and Sottos, N. R., 2007, "Residual Stress Effects on Piezoelectric Response of Sol-Gel Derived Lead Zirconate Titanate Thin Films," *J. Appl. Phys.*, **101**(2), p. 024102.
- Ong, R. J., Berfield, T. A., Sottos, N. R., and Payne, D. A., 2005, "Sol-Gel Derived Pb(Zr,Ti)O₃ Thin Films: Residual Stress and Electrical Properties," *J. Eur. Ceram. Soc.*, **25**, pp. 2247–2251.
- Maiwa, H., Maria, J. P., Christman, J. A., Kim, S. H., Streiffer, S. K., and Kingon, A. I., 1999, "Measurement and Calculation of PZT Thin Film Longitudinal Piezoelectric Coefficients," *Integr. Ferroelectr.*, **24**, pp. 139–146.
- Lefki, K., and Dormans, G. J. M., 1994, "Measurement of Piezoelectric Coefficients of Ferroelectric Thin Film," *J. Appl. Phys.*, **76**(3), pp. 1764–1767.
- Al-Ahmad, M., and Plana, R., 2007, "A Novel Method for PZT Thin Film Piezoelectric Coefficients Determination Using Conventional Impedance Analyzer," Proceedings of the 37th European Microwave Conference, October 2007, Munich, Germany.
- Park, G., Choi, J., Ryu, J., Fan, H., and Kim, H., 2002, "Measurement of Piezoelectric Coefficients of Lead Zirconate Titanate Thin Films by Strain-Monitoring Pneumatic Loading Method," *Appl. Phys. Lett.*, **80**(24), pp. 4606–4608.
- Kholkin, A. L., Wutrich, Ch., Taylor, D. V., and Setter, N., 1996, "Interferometric Measurements of Electric Field-Induced Displacements in Piezoelectric Thin Films," *Rev. Sci. Instrum.*, **67**(5), pp. 1935–1941.
- Chao, C., Wang, Z., and Zhu, W., 2005, "Measurement of Longitudinal Piezoelectric Coefficient of Lead Zirconate Titanate Thin/Thick Films Using a Novel Scanning Mach-Zehnder Interferometer," *Thin Solid Films*, **493**(1–2), pp. 313–318.
- Lee, C.-C., Cao, G. Z., and Shen, I. Y., 2009, "Correlation Improvement between Theoretical and Experimental Results of PZT Thin-Film Membrane Actuators," Proceeding of the ASME 2009 Design Engineering Technical Conference & Computers and Information in Engineering Conference, August 30–September 2, San Diego, CA.